The EMBO Journal (2012) 31, 3718–3729 | © 2012 European Molecular Biology Organization | All Rights Reserved 0261-4189/12
www.embojournal.org

THE EMBO JOURNAL

Positional differences of axon growth rates between sensory neurons encoded by runx3

Francois Lallemend[1,*], Ulrich Sterzenbach[1,4], Saida Hadjab-Lallemend[1,4], Jorge B Aquino[1,5], Goncalo Castelo-Branco[1], Indranil Sinha[1], J Carlos Villaescusa[1], Ditsa Levanon[2], Yiqiao Wang[1], Marina CM Franck[1], Olga Kharchenko[1], Igor Adameyko[1], Sten Linnarsson[1], Yoram Groner[2], Eric Turner[3] and Patrik Ernfors[1,*]

[1]Division of Molecular Neurobiology, Department of Medical Biochemistry and Biophysics, Karolinska Institute, Stockholm, Sweden, [2]Department of Molecular Genetics, The Weizmann Institute of Science, Rehovot, Israel and [3]Center for Integrative Brain Research, Seattle Children's Research Institute, Seattle, WA, USA

The formation of functional connectivity in the nervous system is governed by axon guidance that instructs nerve growth and branching during development, implying a similarity between neuronal subtypes in terms of nerve extension. We demonstrate the molecular mechanism of another layer of complexity in vertebrates by defining a transcriptional program underlying growth differences between positionally different neurons. The rate of axon extension of the early subset of embryonic dorsal root ganglion sensory neurons is encoded in neurons at different axial levels. This code is determined by a segmental pattern of axial levels of Runx family transcription factor Runx3. Runx3 in turn determines transcription levels of genes encoding cytoskeletal proteins involved in axon extension, including Rock1 and Rock2 which have ongoing activities determining axon growth in early sensory neurons and blocking Rock activity reverses axon extension deficits of Runx3$^{-/-}$ neurons. Thus, Runx3 acts to regulate positional differences in axon extension properties apparently without affecting nerve guidance and branching, a principle that could be relevant to other parts of the nervous system.

The EMBO Journal (2012) **31,** 3718–3729. doi:10.1038/emboj.2012.228; Published online 17 August 2012
Subject Categories: neuroscience
Keywords: axon growth; development; intrinsic; Runx3; sensory neurons

*Corresponding authors. F Lallemend or P Ernfors, Division of Molecular Neurobiology, Department of Medical Biochemistry and Biophysics, Karolinska Institute, Scheelesv 1, 17177 Stockholm, Sweden.
Tel.: +46 8524 869 74; Fax: +46 8341 960;
E-mail: francois.lallemend@ki.se or patrik.ernfors@ki.se
[4]These authors contributed equally to this work
[5]Present address: Liver Unit, School of Medicine, Austral University, Av. Peron 1500 (B1629ODT) Derqui-Pilar, Buenos Aires, Argentina and CONICET (Consejo Nacional de Investigaciones Científicas Técnicas)

Received: 22 March 2012; accepted: 20 July 2012; published online: 17 August 2012

Introduction

Extension of axons is an underlying requirement for the establishment of connections between anatomically separated cell populations. During this process, interactions with extrinsic guidance cues imposing attraction and repulsion on the growth cone play a critical role by influencing growth dynamic and direction (Dickson, 2002; Huber *et al*, 2003; O'Donnell *et al*, 2009; Polleux and Snider, 2010). Thus, altering the expression of specific guidance cues has been shown to dramatically affect axon pathfinding. Among others, Ephrins, Semaphorins and growth factors are essential to direct peripheral axon trajectory within the limbs (Huber *et al*, 2005; Kramer *et al*, 2006a; Moret *et al*, 2007; Luria *et al*, 2008). Much of these effects take place by local signalling at the growth cone, although transcriptional mechanisms may also participate. However, in measurement of *in vitro* growth rate of different classes of neurons in Xenopus and mouse, rates between 20 and 75 μm/h have been recorded (Jacobson and Huang, 1985; Davies, 1989) which positively correlate in the mouse with the distance that separates *in vivo* these neurons from their targets, predicting intrinsic differences in the propensity of axonal growth between different neurons (Davies, 1989).

Sensory neurons of the dorsal root ganglia (DRG; Marmigere and Ernfors, 2007) along the vertebral column have different axon lengths depending on the segmental position. Encouraged by the prediction that axon length of pioneering neurons invading peripheral tissue at different axial levels is determined by differences in axon growth rate during development and that such a process is transcriptionally encoded, we examined the developmental process underlying axial differences in nerve growth of the large calibre proprioceptive DRG sensory neurons which are the first to project into the periphery and represent the main sensory component of the nerve trunk during growth into peripheral tissues in early development (Wang and Scott, 2000; Guan *et al*, 2003). These neurons express TrkC and require neurotrophin-3 (NT3) signalling for their survival during the period of naturally occurring cell death (Ernfors *et al*, 1994). NT3 has also been proposed to promote proprioceptive axon growth. However, recent data show that while target invasion and axon branching is critically dependent on nerve growth factor (NGF) and NT3, the nerves reach the target field independently of neurotrophins, suggesting that the growth of the main sensory nerve trunk is a mechanism independent of NGF and NT3 (Lumsden and Davies, 1983; Kucera *et al*, 1995; Patel *et al*, 2000, 2003; Genc *et al*, 2004; Wickramasinghe *et al*, 2008). Here, we demonstrate that DRG neurons of different axial levels display differences in growth rates at the time when nerves invade the limbs, and that such difference is encoded by graded levels of the transcription factor Runx3 which controls the expression of cytoskeletal proteins and Rock proteins participating in axon growth.

Results

Axial differences in the rate of sensory neuron nerve growth

We first addressed whether there is an *in vivo* difference in axon growth rate between pioneering neurons growing into limbs or non-limb trunk axial levels. Chick embryos were collected with 6 h intervals between HHst25 and 27 and stained for Axonin-1 which specifically recognized sensory axons at these stages (Figure 1A, Hamburger-Hamilton stage (HHst) 27 chick embryo) (Honig *et al*, 1998). The growth rate was 41 μm/h for thoracic nerves and 63 and 83 μm/h for forelimb and hindlimb nerves, respectively, showing that nerves of different axial levels display different growth rates *in vivo*. We next determined if these positional differences are inherent to the neurons by examining if isolated neurons placed in a context independent of environmental cues (secreted locally or along the nerve tracts) show similar differences in axon growth than that observed *in vivo*. In low-density *in vitro* cultures, brachial, lumbar and thoracic neurons retained the differential growth behaviour observed *in vivo* when placed *in vitro* with brachial and lumbar DRG neurons exhibiting significantly greater rates of axon growth than those from thoracic region (Figure 1B and C; Supplementary Figure S1A, HHst27). No difference in soma diameter was observed between neurons from different axial levels ($P>0.05$). Furthermore, axon growth was unaffected by growth factors at these early stages (Supplementary Figure S1B). Similar results, i.e., greater axon growth rate at limb than at thoracic levels, were obtained with DRG neurons cultured from HHst26 ($P<0.01$) and late HHst27 ($P<0.001$).

A strict temporal, spatial and cellular correlation of Runx3 with different capacities for nerve growth

The transcription factor Runx3 appeared as a possible underlying candidate factor encoding intrinsic axial differences in axon growth rate because Runx3 and the related transcription factor Runx1 affect axon termination patterns in the spinal cord, axon growth of differentiated neural stem cells *in vitro* (Chen *et al*, 2006; Marmigere *et al*, 2006) and are involved in the diversification of sensory neurons (Levanon *et al*, 2002; Kramer *et al*, 2006b). Strikingly, at HHst27, Runx3 mRNA as determined by *in situ* hybridization (Figure 1D and E), quantitative PCR (qPCR) (Figure 1F) and protein levels (Figure 1G and H) displayed differential expression along the rostro-caudal axis with overall less expression as well as lower levels per cell in cervical and thoracic as compared to brachial and lumbar DRG, similar to the limb-induced ETS transcription factor PEA3 (Lin *et al*, 1998; Supplementary Figure S2A). In contrast, the Runx3 cofactor CBFβ, β-actin and TrkC exhibited similar expression at all segmental levels (Supplementary Figure S2B–F). Runx1, a key transcription factor for cutaneous ($TrkA^+$) sensory neurons, was very low until E7 (HHst31; Supplementary Figure S2I) consistent with that these neurons are born and project into the nerves later in development than proprioceptive $TrkC^+$ neurons (Guan *et al*, 2003). The close spatial correlation of Runx3 and axon

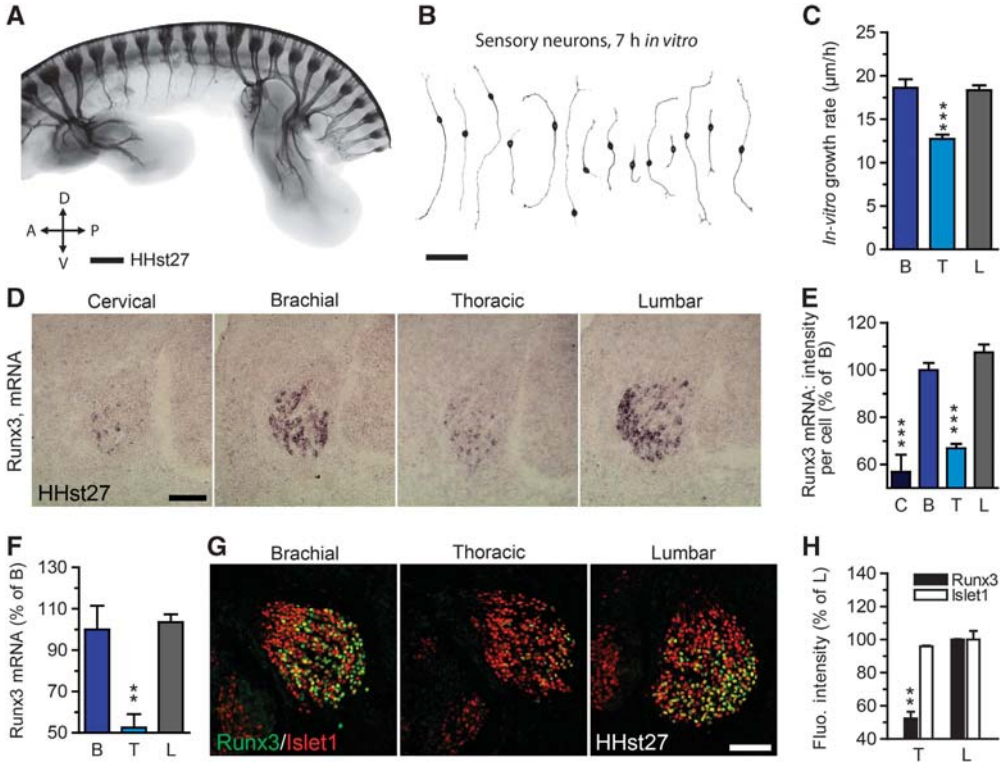

Figure 1 Differential DRG axon growth along the rostro-caudal axis correlates with Runx3 expression. (**A**) Whole-mount Axonin-1 immunostaining of an HHst27 chick embryo showing the positional differences in sensory axon growth. (**B**) Differential outgrowth of cultured HHst27 DRG neurons. (**C**) Axon growth rate of HHst27 DRG neurons ($n=12$). (**D**) Runx3 mRNA expression at different axial levels. (**E**) Quantification of (**D**) ($n=3$ embryos). (**F**) Quantitative (q)PCR analysis of Runx3 mRNA levels in HHst27 DRG ($n=4$). (**G**, **H**) Runx3 protein levels at different axial levels ($n=2$). C, cervical; B, brachial; T, thoracic; L, lumbar. (**C**, **E**, **F**) One-way ANOVA with Tukey's *post hoc* test, statistical comparison with brachial; (**H**) two-tailed, unpaired *t*-test. Mean ± s.e.m; $^{**}P<0.01$, $^{***}P<0.001$. Scale bars: (**A**) 0.5 mm; (**B**) 80 μm; (**D**, **G**) 100 μm.

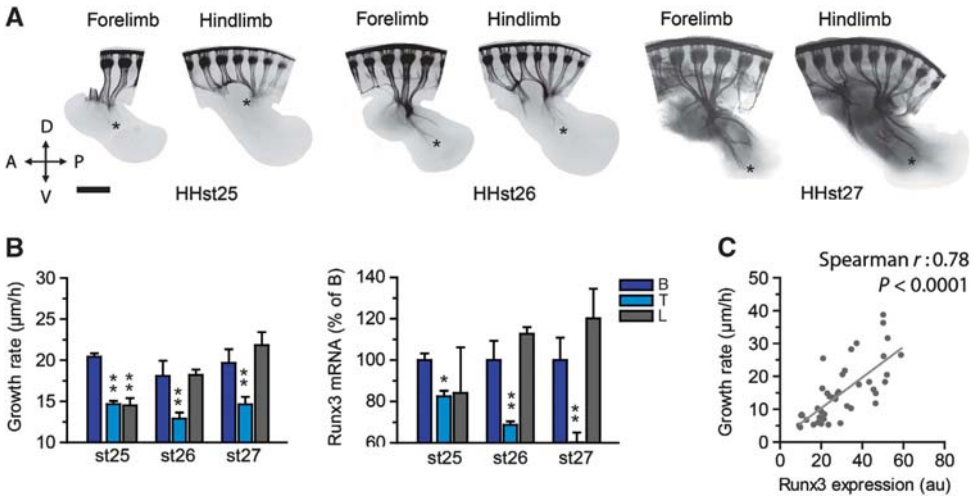

Figure 2 Temporal, spatial and cellular correlation of Runx3 with capacity of nerve growth. (**A**, **B**) Temporal and axial aspects of Axonin-1$^+$ sensory axon growth within the limbs (**A**, asterisks) correlate with growth property in cultures ($n=7$) (**B**) and the levels of Runx3 expression assessed by qPCR (**B**) ($n=4$). (**C**) Correlation between axon growth rate and level of Runx3 expression in individual neurons of brachial HHst26 DRG. B, brachial; T, thoracic; L, lumbar. (**B**) One-way ANOVA with Tukey's *post hoc* test, statistical comparison with brachial (mean ± s.e.m; $*P<0.05$, $**P<0.01$). Scale bar: (**A**) 0.5 mm.

growth encouraged us to perform a detailed correlation also of temporal aspects of sensory nerve growth *in vivo* at different trunk levels between HHst25 and HHst27 (Figure 2A) with that of Runx3 expression (Figure 2B; Supplementary Figure S2G) and *in vitro* axon growth (Figure 2B). This study revealed a direct temporal correlation of increased Runx3 expression and increased *in vitro* growth behaviour with actual invasion of brachial and lumbar nerves into the limbs *in vivo*, while Runx3 levels and axon growth at the thoracic level remained unchanged between HHst25 and 27. These results show that Runx3 is elevated in sensory neurons at limb levels at a time when their axons approach the limb mesenchyme and such increase closely correlates with axon growth behaviour. Strikingly, this finding extended to individual cells as correlating Runx3 protein level and axon growth in single neurons from HHst26 brachial DRG revealed a close and significant correlation between the level of Runx3 and axon extension (Figure 2C).

Axial differences of Runx3 expression and axon growth independent of the peripheral target

The parsimonious explanation for the increased growth and Runx3 levels at limb levels is the presence of limb-derived signals instructing enhanced growth behaviour. We therefore next addressed if the axial differences of Runx3 expression and axon growth were determined by signals emanating from the target. Animals with unilateral ablation of hindlimb buds long before the onset of axon outgrowth (HHst18) (Figure 3A; Caldero *et al*, 1998) were analysed at HHst26 to late HHst27, the last developmental stage allowing for analysis, since at later stages target deprivation-induced cell death of DRG neurons occurs (Caldero *et al*, 1998). No difference in the pan sensory neuron marker Isl1, TrkC or CBFβ mRNA expression was seen in lumbar DRG ipsilateral to the ablation using qPCR (Supplementary Figure S3A–C), showing that ablation did not affect neuronal survival at the analysed stage. In contrast, PEA3 mRNA expression was reduced to a level comparable to that observed at the thoracic level (Figure 3B; lumbar + ablation: 55.71 ± 12.07%, thoracic: 56.07 ± 12.13%, in % of lumbar), consistent with previous data showing its dependence on the target for expression (Lin *et al*, 1998). Unexpectedly, neither Runx3 mRNA expression nor protein levels were affected by the ablation (Figure 3C–E). Furthermore, ablation did not affect the nerve extension exhibited by late HHst27 lumbar DRG in low-density cultures (Figure 3F). The persistence of Runx3 expression and nerve outgrowth in lumbar DRG was also observed after performing both hindlimb and tail buds ablation, a procedure that eliminates any other alternative source of target-derived signals (growth rate from lumbar DRG neurons (μm/h): control, 23.58 ± 2.56; hindlimb and tail buds ablation, 24.83 ± 4.46; $P>0.05$) (Caldero *et al*, 1998). Taken together, these results provide evidence that the axial differences of Runx3 expression are determined independently of the peripheral target at these stages.

Axial differences in axonal growth functionally determined by Runx3

The segmental-specific patterning of Runx3 levels in DRG correlating with their growth properties when nerves enter the limbs prompted us to functionally address its role for determining axon growth behaviour. Runx3 activity was attenuated in sensory neurons by electroporating HHst13–14 embryos with a Runx1d construct interfering with Runx activity (pCARunx1d) and green fluorescent protein (eGFP) reporter plasmid which effectively leads to expression of these delivered constructs in DRG neurons (Marmigere *et al*, 2006). Runx1d is an endogenous isoform of 243 amino acids that binds to DNA but is not capable of transactivation and therefore interferes with the activity of all three mammalian Runx proteins due to its higher affinity for the consensus binding site (Bae *et al*, 1994; Meyers *et al*, 1995; Tanaka *et al*, 1995b). Runx1d is expected to selectively block Runx3 activity, since only Runx3 is expressed in the DRG at the studied stages (Supplementary Figure S2G and I; Chen *et al*, 2006). Lumbar HHst26 eGFP$^+$/βIII-tubulin$^+$

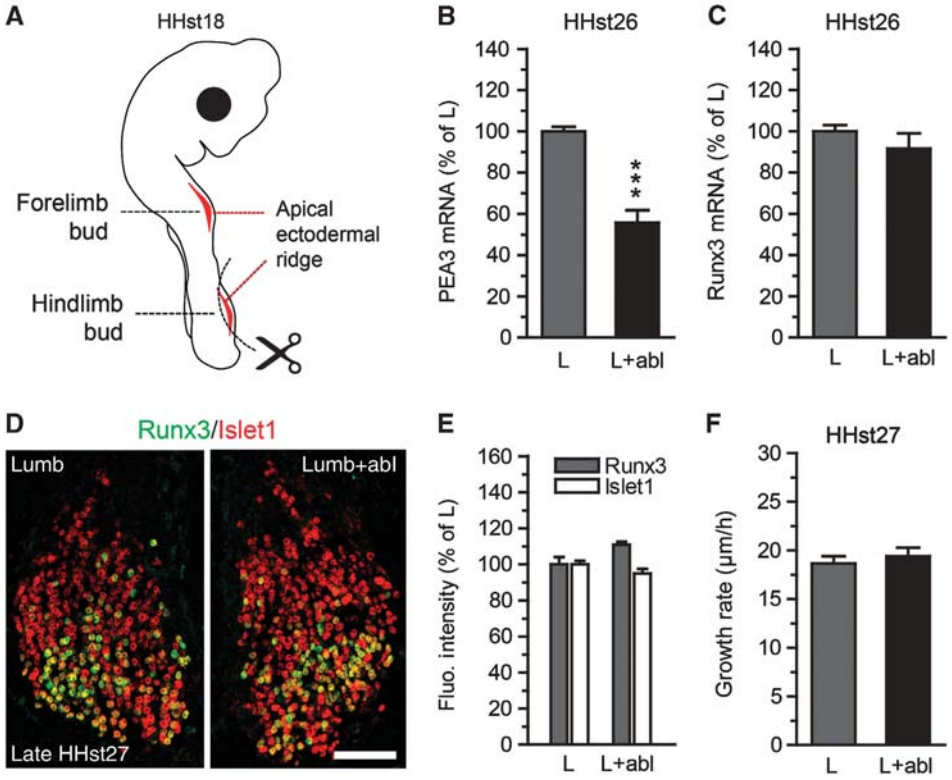

Figure 3 The establishment of axial differences of Runx3 expression in DRG neurons is independent of limb-derived signals. (**A**) Schematic of HHst18 hindlimb bud ablation. (**B**, **C**) Quantification of PEA3 (**B**) and Runx3 mRNA (**C**) in HHst26 lumbar DRG from ipsilateral (L + abl) and contralateral (L) sides of hindlimb bud ablation ($n = 4$). (**D**) Runx3 protein in late HHst27 lumbar DRG is similar after ablation (L + abl compared to L). (**E**) Quantification of (**D**) confirming target independence of Runx3 protein levels. Note also that the expression of Isl1 in neurons is similar on both sides ($n = 3$ embryos). (**F**) Mean axon growth rate in dissociated cultures of lumbar HHst27 DRG neurons from ipsilateral and contralateral side after ablation ($n = 10$). Note that growth properties of HHst27 axons from lumbar DRG neurons are unaffected by the absence of the limb. (**B**, **C**, **E**, **F**) Mean ± s.e.m.; $***P < 0.001$, two-tailed, unpaired *t*-test. Scale bar: 80 µm.

neurons that show a strong axon growth and Runx3 expression at this stage were analysed by measuring axon growth after 7 h *in vitro*. pCARunx1d expression led to a significant decrease in axon growth compared to controls (Figure 4A). Similar results were obtained with brachial DRG neurons (growth rate (µm/h): control, 20.58 ± 4.89; pCARunx1d, 9.37 ± 3.9; $P < 0.001$). Soma diameters of transfected neurons were similar in both conditions ($P > 0.05$). Moreover, while distance to the first branch was not affected by pCARunx1d transfection, fewer sensory neurons exhibited at least one arborization in the experimental condition compared to controls (Figure 4B; Supplementary Figure S4A). This shows that Runx activity does not affect branching and that the effect on axon elongation is not a secondary consequence of increased and/or precocious branching. Addition of neurotrophins did not affect axon outgrowth in control or pCARunx1d-transfected DRG neurons (Supplementary Figure S4B). Reducing endogenous Runx3 mRNA levels in sensory neurons by siRNA affected axon length similarly as the dominant-negative construct (Figure 4C and D; Supplementary Figure S4C) confirming a Runx3-dependent growth of axons. We next increased Runx3 expression using a pCARunx3 construct in sensory neurons having short axons and low levels of endogenous Runx3 (i.e., HHst25 thoracic neurons). pCARunx3 led to a two-fold increase in axon growth compared to controls (Figure 4E; Supplementary Figure S4D). Hence, reducing Runx3 in neurons with strong axon growth (i.e., lumbar neurons) reduced axon elongation resembling thoracic neurons with weak axon growth while increasing Runx3 in neurons with low levels changed growth behaviour to strong axon growth. In contrast, transfection of HHst25 thoracic neurons with pCARunx1d construct, which impedes Runx activity, did not affect axon growth compared to controls cells (growth rate (µm/h): control, 13.66 ± 4.42; pCARunx1d, 9.60 ± 2.38; $P > 0.05$), indicating that Runx3 affects axon growth specifically above a certain basal level. These results do not address whether Runx3 acts as a binary on-off switch to induce axon elongation or in a level-dependent fashion which would be predicted from the observation of diverse levels of Runx3 immunoreactivity in the sensory neuron population that are correlated with their axon growth (Figure 2C). The pCMV promoter driving eGFP led to 40% less GFP intensity but unchanged numbers of transfected neurons when compared to pCAeGFP-transfected neurons (Figure 4F; Supplementary Figure S4E–G). Expression of a pCMVRunx1d construct in brachial and lumbar sensory neurons had intermediate effects on axon growth compared to control-transfected (pCAeGFP) and pCARunx1d-expressing neurons (Figure 4G). Analysis of the distribution of the axon length in these cultures showed a general shift towards shorter axon length without any bimodal distribution, indicating an effect on most sensory neurons (Supplementary

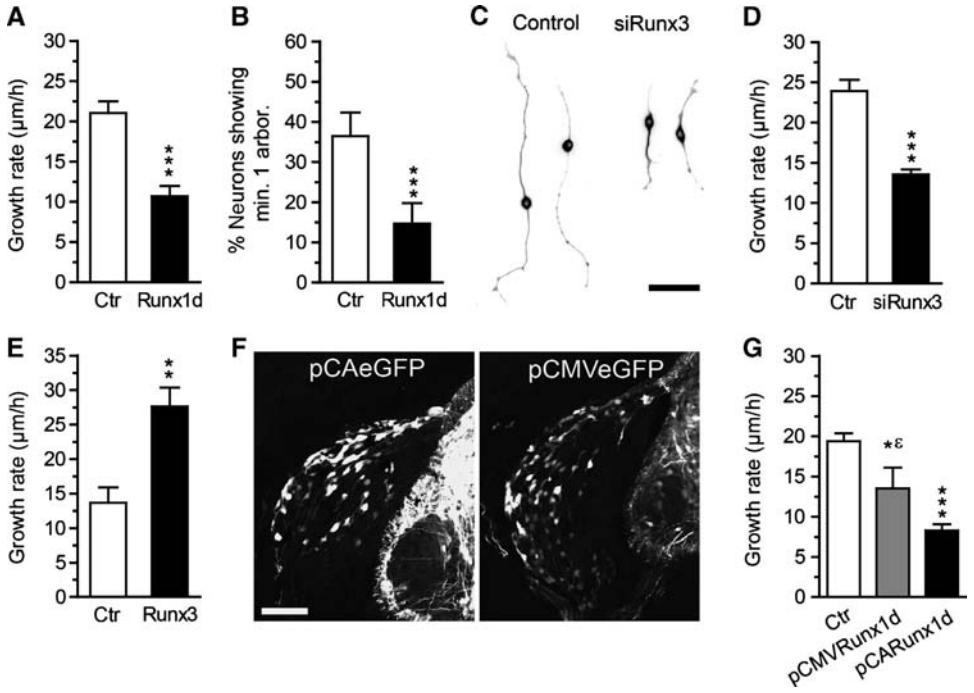

Figure 4 Runx3 levels determine axial differences of sensory axon elongation. (**A**–**D**) Axon growth (**A**, **C**, **D**) and arborization (**B**) of HHst26 brachial sensory neurons from control (Ctr) or Runx1d (**A**, **B**) or Runx3 siRNA (**C**, **D**) in ovo-transfected DRG ($n = 6$–11). (**E**) Increasing Runx3 levels by pCARunx3 expression in thoracic DRG neurons of HHst25 embryos results in increased axon growth ($n = 4$). (**F**) Expression of eGFP in DRG and half neural tube in pCAeGFP- and pCMVeGFP-transfected embryos analysed at HHst26. Note similar number of neurons but lower expression of eGFP using *pCMV* compared to *pCA* promoter. (**G**) Axon growth of HHst26 brachial sensory neurons from pCARunx1d- or pCMVRunx1d-in ovo-transfected DRG cultured for 7 h (statistical comparison with control* or with pCARunx1d$^{\varepsilon}$). (**A**, **B**, **D**, **E**) Two-tailed, unpaired *t*-test and (G) one-way ANOVA with Tukey's *post hoc* test. Mean ± s.e.m.; $^{*}P<0.05$, $^{\varepsilon}P<0.05$, $^{**}P<0.01$, $^{***}P<0.001$. Scale bars: (**C**) 80 μm; (**F**) 100 μm.

Figure S4H). Taken together, these results suggest that graded activities of Runx3 determine axon growth rate of sensory neurons from different axial levels.

A physiological role of Runx3 for nerve elongation in vivo

Using mouse genetics, we next addressed if Runx3 activity influences the growth of sensory axons *in vivo*. We observed in mouse embryos a similar correlation of Runx3 levels and axon growth at E11.5 and E12.5 when brachial DRG neurons initiate growth into the forelimb, as described in chick. Runx3 levels per neurons were significantly greater in brachial as compared to thoracic DRG (Figure 5A and B; Supplementary Figure S5A and B). This difference correlated with axon growth behaviour *in vitro* using ganglion explant cultures in matrigel, a substrate that permits outgrowth of sensory axons *in vitro* independently of neurotrophins (Graef *et al*, 2003; Supplementary Figure S5C and D). We observed, similar to the chick, a positional difference in axon growth in the mouse where E11.5 wild-type (WT) thoracic DRG displayed significantly shorter axons than brachial DRG (Figure 5C and D). Furthermore, at the time of initiation of growth into the limbs in the mouse, i.e., E11.5, DRG neurons were mostly Runx3^{+}, while later born neurons express TrkA and Runx1 (starting at E12.5) (Kramer *et al*, 2006b). By analysing axon growth of Runx3^{-}/TrkA^{+} neurons at E12.5, a stage when there are both Runx1/TrkA and Runx3/TrkC neurons in the DRG, mechanoreceptive (including TrkC^{+} proprioceptive) axons which are Neurofilament 160 kD^{+} (2H3^{+})/βIII-tubulin, and nociceptive (TrkA^{+}) axons which are βIII-tubulin^{+} but negative for neurofilament 160 kD (2H3 antibody) were growing in very close association, but the longest axons were invariably negative for TrkA, an observation that was quantitatively confirmed (Supplementary Figure S5E–G). Hence, Runx3^{+} neurons that are born early in the DRG display faster axon growth than Runx1/TrkA neurons, and also represent the pioneering axons invading the limb (Guan *et al*, 2003).

We next examined if Runx3 is the critical regulator of axial differences in axon growth between limb and thoracic sensory neurons in the mouse. In E11.5 Runx3$^{-/-}$ mice, axon growth of brachial neurons was markedly reduced and comparable to WT thoracic DRG (Figure 5E and F, $P>0.05$). Hence, this shows that axial difference in axon growth was abolished in Runx3$^{-/-}$ mice. Cell survival was not affected in these animals at the analysed stage, i.e., E11.5 (Supplementary Figure S6A and B) and no sign of increased cell death was observed in culture as assessed by quantification of active caspase-3^{+} cells ($P>0.05$). Combined, these results confirm that Runx3 is the critical mediator of differences in axon growth *in vitro*. To investigate the role of Runx3 in peripheral sensory axon elongation *in vivo*, we carried out whole-mount immunofluorescent staining of Runx3$^{-/-}$ mice using antibodies directed against neurofilament (2H3) and TrkC to identify axons of neurons normally expressing Runx3 (Levanon *et al*, 2002). Although the level of TrkC immunoreactivity is decreased in the mutant mice, as previously reported (Levanon *et al*, 2002; Kramer *et al*, 2006b), it was still clearly visible (Supplementary

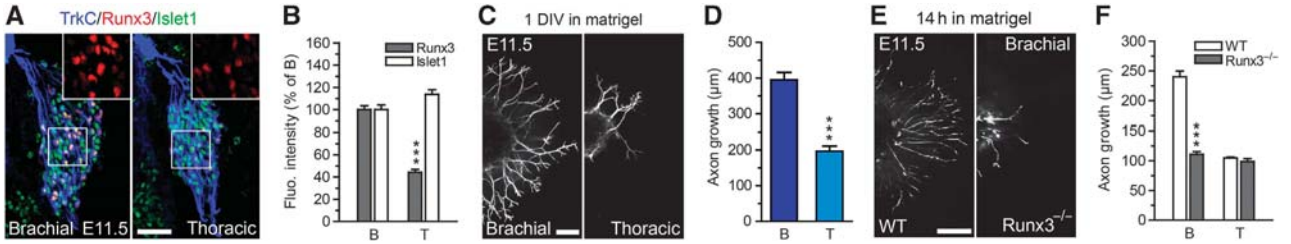

Figure 5 Axial differences in axon growth behaviour established by Runx3 in the mouse. (**A**) Immunohistochemistry for Runx3 in E11.5 brachial (**B**) compared to thoracic (T) DRG neurons. (**B**) Quantification of Runx3 and Isl1 at single cell level of (**A**) ($n=2$ embryos). (**C**) Axon growth differences of E11.5 brachial and thoracic mouse DRG (1 DIV). (**D**) Quantification of (**C**) ($n=6$). (**E**) Axon growth of E11.5 brachial DRG from WT and Runx3$^{-/-}$ mice (14 h). (**F**) Quantification of axon growth of E11.5 brachial and thoracic DRG from WT and Runx3$^{-/-}$ mice (14 h) ($n=10$ and 15). (**B**, **D**, **F**) Two-tailed, unpaired *t*-test. Mean ± s.e.m.; ***$P<0.001$. Scale bars: (**A**) 40 μm; (**C**) 100 μm; (**E**) 130 μm.

Figure S6A) and enabled a detailed assessment of the peripheral projections of muscle DRG neurons (Figure 6A). Analysis of E12.5 Runx3$^{-/-}$ embryos revealed no difference in the initial extension of these axons towards the nerve plexus but a severe reduction in sensory axon elongation into the limbs (Figure 6A). The Brn3a$^{+/TLZ}$ locus express a genetic axonal tracer, Tau/β-galactosidase in the Brn3a locus that provides means for visualization of sensory neuron projections (Quina *et al*, 2005). We generated Runx3$^{-/-}$;Brn3a$^{+/TLZ}$ mice to genetically allow visualization specifically of sensory (but not motor) axon projections. Runx3$^{-/-}$;Brn3a$^{+/TLZ}$ embryos formed nerve trunks up to the brachial plexus, but elongation of sensory axons past plexus was significantly reduced (Figure 6D). Mice lacking Runx3 started to show increased numbers of apoptotic cells in brachial DRG neurons at E12.5 (Supplementary Figure S6B) and at E13.5 there was a massive loss of Runx3-expressing neurons as determined by β-galactosidase activity from the LacZ gene inserted into the Runx3 locus (Supplementary Figure S6C; Levanon *et al*, 2002). The deletion of the proapoptotic gene Bax rescues sensory neurons from death and affords the unique ability to study survival-independent processes in sensory neurons (White *et al*, 1998; Patel *et al*, 2003). Consistently, the neuronal loss could be prevented by crossing the Runx3$^{+/-}$ mice to Bax$^{+/-}$ mice, generating Runx3$^{-/-}$;Bax$^{-/-}$ mice (Supplementary Figure S6C). We therefore crossed all three alleles to generate Runx3$^{-/-}$;Bax$^{-/-}$;Brn3a$^{+/TLZ}$ mice. Analysis of such mice allowed us to address the role of Runx3 specifically in sensory axon growth in the developing mouse *in vivo* independent of neuronal survival. Runx3$^{-/-}$;Bax$^{-/-}$;Brn3a$^{+/TLZ}$ mice displayed similar defects of axon growth as seen in Runx3$^{-/-}$;Brn3a$^{+/TLZ}$ littermates (Figure 6B–D). Conflicting results have been obtained on the role of Runx3 for specification of proprioceptive neurons as determined by TrkC expression (Inoue *et al*, 2002; Levanon *et al*, 2002). Our results show that these data could be confounded by the death of Runx3-expressing neurons that starts at E12.5 in mice (Supplementary Figure S6B). We used the compound Runx3$^{-/-}$;Bax$^{-/-}$ mice also to resolve Runx3-mediated effects on cell type specification. Normal numbers of TrkC^{+} neurons were formed although levels of TrkC expression per cell were reduced in Runx3$^{-/-}$;Bax$^{-/-}$ mice (Figure 6E and F), suggesting that Runx3 is not necessary for the formation of TrkC^{+} neurons. The effect of an absence of Runx3 on axon growth is therefore not secondary to a failure of development or survival of TrkC^{+} neurons.

We analysed the presence of muscle spindles in Runx3$^{-/-}$;Bax$^{-/-}$ hindlimb skeletal muscles at E18.5. Muscle spindles are peripheral end organs innervated by proprioceptive neurons, and their development starting at E15.5–16.5 depends on the presence of proprioceptive afferents as they contact nascent intrafusal muscle fibres (Kucera *et al*, 1995; Hippenmeyer *et al*, 2002). Muscle spindles, revealed by expression of the ETS transcription factor PEA3 (Hippenmeyer *et al*, 2002), were clearly identified on cross-sections of hindlimb muscles of Bax$^{-/-}$ mice (Figure 6G), regardless of the proximo-distal position in the lower limb. In striking contrast, we found a complete absence of muscle spindles in hindlimb muscles of Runx3$^{-/-}$;Bax$^{-/-}$ mice (Figure 6G). This strongly suggests that the early failure of proprioceptive axons to elongate their peripheral projections within the limb results in a loss of contact with myotubes and therefore a failure of muscle spindle induction. This conclusion was corroborated by examining expression of the ETS transcription factor ER81, which is induced in sensory neurons by the target, i.e., the muscle (Patel *et al*, 2003). E13.5 Runx3$^{-/-}$;Bax$^{-/-}$ mice showed a complete loss of ER81 expression in DRG neurons, as compared to control Bax$^{-/-}$ embryos (Supplementary Figure S7).

E11.5 brachial DRGs of WT and Runx3$^{-/-}$ mice were dissected and RNA transcripts were sequenced for whole transcriptome analysis to reveal underlying molecular mechanism of Runx3 activity on axon growth. Analysis of gene activity with >1.25-fold change revealed 422 and 477 genes with increased and decreased expression, respectively. Functional annotation category clustering using DAVID (Huang da *et al*, 2007a, b; Sherman *et al*, 2007; Supplementary Figure S8; Supplementary Tables S1 and S2) identified among genes dependent on Runx3 for normal expression an enrichment in gene ontology categories reflecting cytoskeleton/morphogenesis processes as the top categories (Figure 6H). Of the 52 downregulated genes (Supplementary Table S3) in the five most enriched categories, 26 were associated with axon growth/cell migration and 15 of these encoded genes directly involved in actin-microtubule cytoskeleton/dynamics (Figure 6I; Supplementary Tables S4 and S5), showing that Runx3 controls expression levels of cytoskeletal structural components. Categories of genes suppressed by Runx3 were primarily cell cycle related, among which 29 genes were associated with cytoskeleton-related genes participating in cell cycle (Supplementary Tables S6 and S7). Within these genes, 13 were associated with axon growth/cell migration (Supplementary Table S7). This category also included Ntrk2 (encoding TrkB) previously known to be suppressed by Runx3 (Kramer *et al*, 2006b) and Rho-kinase (Rock) 1 and Rock2. We examined for regulation of other genes in the Rock pathway

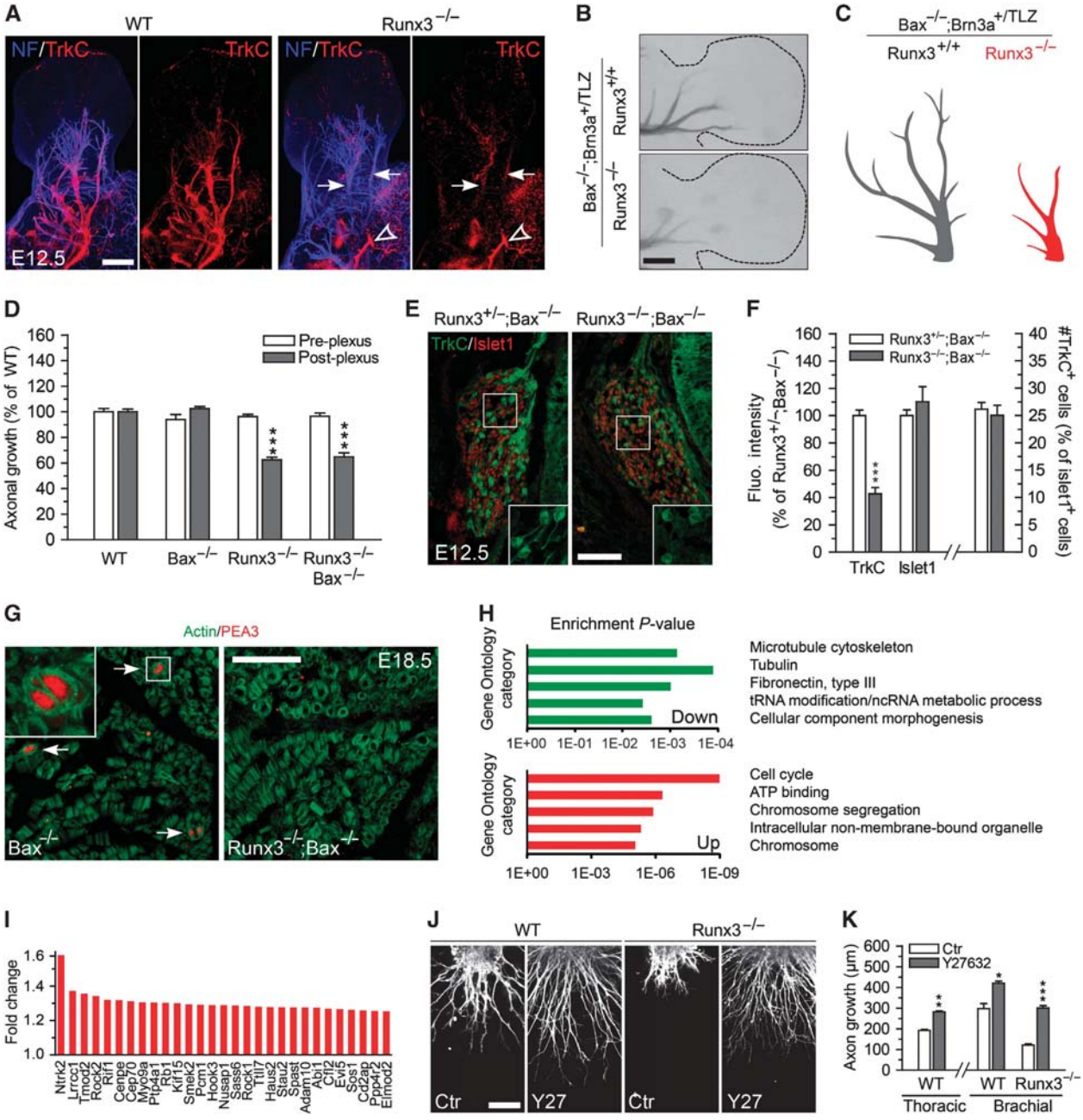

Figure 6 Runx3 is required for peripheral axon elongation *in vivo* in the mouse. (**A**) Impairment of TrkC$^+$ and neurofilament$^+$ (NF$^+$) projections in E12.5 Runx3$^{-/-}$ embryos (arrows point at few TrkC$^+$ fibres) compared to wild-type (WT). (**B**) Forelimbs from whole-mount E12.5 Runx3$^{+/+}$;Bax$^{-/-}$;Brn3a$^{+/TLZ}$ and Runx3$^{-/-}$;Bax$^{-/-}$;Brn3a$^{+/TLZ}$ embryos stained for β-gal activity. (**C**) Schematic drawings depicting the dramatic defect in (**B**). (**D**) Quantification of *in vivo* axon growth in Runx3$^{-/-}$ and Runx3$^{-/-}$;Bax$^{-/-}$ mice ($n=3$–6 animals, statistical comparison with WT). (**E**) Immunostaining showing that TrkC expression is decreased in E12.5 DRG neurons in the absence of Runx3 (and Bax). (**F**) Quantification of the immunostaining showing decreased immunoreactivity for TrkC in DRG neurons from Runx3$^{-/-}$; Bax$^{-/-}$ compared to Runx3$^{+/-}$;Bax$^{-/-}$ embryos. Note that the expression of Isl1 in neurons and that the number of TrkC$^+$ neurons is similar in both genotypes ($n=2$ embryos, as percentage of Runx3$^{+/-}$;Bax$^{-/-}$). (**G**) Analysis of muscle spindle formation by immunostaining of PEA3 at E18.5 on cross-section of soleus muscle from Bax$^{-/-}$ and Runx3$^{-/-}$;Bax$^{-/-}$ embryos. Arrows mark nascent muscle spindles, as seen at higher magnification in the inset. (**H**) The five gene ontology categories with greatest enrichment in down (green) and up (red) regulated genes of Runx3$^{-/-}$ compared to WT E11.5 DRG following RNA sequencing analysis. (**I**) Average fold increase in expression of the 29 Runx3-dependent cytoskeleton related genes included within the cell-cycle gene ontology category shown in (**H**). (**J**) Axon growth of brachial DRG from E11.5 WT and Runx3$^{-/-}$ mice. (**K**) Quantification of axon growth of E11.5 DRG cultured for 14 h *in vitro* in the presence or absence of the Rock inhibitor Y27632 (30 μM) ($n=10$–15). Note marked elevation of growth of thoracic neurons and that deficit of axon growth of brachial neurons from Runx3$^{-/-}$ mice is largely rescued by Y27632. (**D**) One-way ANOVA with Tukey's *post hoc* test and (**F**, **K**) two-tailed, unpaired *t*-test. Mean ± s.e.m.; $^*P<0.05$, $^{**}P<0.01$, $^{***}P<0.001$. Scale bars: (**A**) 280 μm; (**B**) 300 μm; (**E**) 100 μm; (**G**) 80 μm; (**J**) 100 μm.

and identified protein phosphatase 1 (PP1) regulatory subunit 12C (PPP1R12C, 0.82% of control), which is a myosin phosphatase targeting subunit of PP1 that decreases phosphorylation of and inactivates NMII (Bannert *et al*, 2003; Vicente-Manzanares *et al*, 2009). Hence, Rock1 and Rock2 that phosphorylate and activate NMII are increased

and PPP1R12C, which dephosphorylates and inactivates NMII, is decreased in Runx3$^{-/-}$ mice. An ongoing Rock activity which inhibits axon growth that is suppressed by Runx3 therefore appeared as a possible underlying mechanism. Inhibition of Rock activity by Y27632 (30 μM) led to a significant increased axon growth of thoracic DRG neurons (Figure 6K), consistent with the presence of an ongoing Rock activity restricting axon growth at this stage in development. Furthermore, blebbistatin, a selective inhibitor of NMII (Kovacs *et al*, 2004) caused a marked increase in axon length (axon growth of E11.5 thoracic DRG neurons: control, 100 ± 9.79; blebbistatin (10 μM), 128.55 ± 2.89; in % of control, $P<0.01$). To assess whether alteration in the Rock-NMII pathway directly participates in the Runx3$^{-/-}$ axon growth phenotype, E11.5 brachial DRG from WT and Runx3$^{-/-}$ mice were cultured for 14 h in the presence or absence of Y27632. Inhibition of Rock activity rescued the axon growth deficits of brachial Runx3$^{-/-}$ neurons to a level comparable to that of WT DRG neurons (Figure 6J and K). This suggests that Runx3 inhibits an ongoing Rock activity and that this inhibition leads to increased axon growth properties.

Discussion

Previously, a few transcriptional regulators of axon extension have been identified in vertebrates and these appear to control axon pathfinding and responsiveness to environmental cues and consequently, mutant mice display deficits in nerve trajectories (Kania *et al*, 2000; Sharma *et al*, 2000; De Marco Garcia and Jessell, 2008). In this report, we demonstrate that Runx3 acts as a regulator of axon growth encoding positional information of sensory neurons at different axial levels in chick and mouse. This positional information by Runx3 appears encoded locally in progenitors, suggesting that local organizing morphogens instruct positional information during nervous system development that influence axon growth behaviour of pioneering sensory neurons at later developmental stages. This conclusion is evidenced by the existence of a 'memory' of axial differences in growth behaviour along the rostrocaudal axis defined by Runx3 levels. The encoding of these differences might not be cell autonomous and likely involves instructive molecules that may arise from nervous tissue or adjacent mesodermal tissue but is not target dependent, as limb ablation did not affect growth behaviour or Runx3 expression. The significance of this finding is underscored by the fact that the growth rate was comparable across different axial levels in cells with reduced/absence of endogenous Runx3 both *in vitro* and *in vivo* in the chick and mouse and furthermore, by the finding that elevated Runx3 in non-limb trunk neurons convert their growth behaviour to that of limb neurons.

Large-size proprioceptive neurons are born before small size thermosensitive, pruritogenic and nociceptive sensory neurons. Large neurons are complete in numbers in mouse already at late E10 (HHst25 in chick) while small size neurons continue to be generated by cell division until E12.5 (HHst28 in chick) (Lawson and Biscoe, 1979; Montelius *et al*, 2007; Bachy *et al*, 2011). Consequently, pioneering axon growth is represented by large neurons (Guan *et al*, 2003). Runx3 is expressed in large-size neurons starting already at the time of neurogenesis (i.e., E10.5 at brachial level in mouse) (Levanon *et al*, 2002) and our data show that a large proportion of the DRG neurons express Runx3 in the DRG up to HH27 in the chick and E11.5 in the mouse. Thus, we conclude that the axial difference in axon growth is manifested by pioneering large-size neurons and within these neurons it is governed by Runx3. The independence of axon growth from the target as well as from neurotrophins is consistent with recent data showing that while target invasion and axon branching critically depend on NGF and NT3, the nerves reach the target field independently of neurotrophins, suggesting that the growth of the main sensory nerve trunks is a mechanism independent of NGF and NT3 (Lumsden and Davies, 1983; Kucera *et al*, 1995; Patel *et al*, 2000, 2003; Genc *et al*, 2004; Wickramasinghe *et al*, 2008).

Runx3 has been implicated as a critical transcriptional determinant defining specification of TrkC^{+} proprioceptive DRG neurons (Inoue *et al*, 2002; Levanon *et al*, 2002; Kramer *et al*, 2006b). However, by crossing Runx3$^{-/-}$ mice to Bax$^{-/-}$ mice we were able to dissociate the role of Runx3 for neuronal survival and for specification. These results show that TrkC^{+} neurons are generated in normal numbers independent of Runx3 in compound Runx3$^{-/-}$;Bax$^{-/-}$ mice at E12.5. Runx3 has also been proposed to regulate proprioceptive neuron axon termination patterns in the chicken spinal cord (Chen *et al*, 2006) since reducing Runx3 in the chick caused sensory axon terminations in intermediate instead of the ventral region of the spinal cord (Chen *et al*, 2006). However, our results raise the question whether Runx3 is directly involved in establishing central termination patterns. As proprioceptive axons invade the peripheral target, factors in the muscle induce ER81 (Lin *et al*, 1998; Patel *et al*, 2003). Expression of ER81 in sensory neurons is necessary for their central projections to grow past the intermediate spinal cord (Arber *et al*, 2000). In this way, the muscle defines central termination patterns of proprioceptive afferents. We find a complete absence of muscle spindles in hindlimb muscles in Runx3$^{-/-}$;Bax$^{-/-}$ mice suggesting that proprioceptive afferents failed to innervate their peripheral target muscles in these mice, therefore resulting in their inability to project centrally. ER81$^{-/-}$ mice display deficits of central but not of peripheral sensory projections (Arber *et al*, 2000). We find that expression of ER81, normally induced by the peripheral target field at E13 in mouse (Arber *et al*, 2000), is virtually absent at E13.5 in DRG from Runx3$^{-/-}$;Bax$^{-/-}$ mice. Thus, Runx3-related deficits of central projections in mouse may be secondary to its effects on peripheral innervation and ER81 expression (Arber *et al*, 2000). Hence, based on the results in this study, we believe that one main function of Runx3 during early development of sensory neurons is represented by its role defining axial differences in axon growth.

Our results suggest that regulation of axon growth by Runx3 is complex and likely involves multiple mechanisms; based on whole transcriptome analysis, structural as well as regulatory components of microtubule and actin represent a major category of Runx3-regulated genes. Since the rate of microtubule extension and rate of axon growth are reflected by the status of actin and microtubule configurations (Tanaka and Kirschner, 1991; Tanaka *et al*, 1995a; Conde and Caceres, 2009), such changes in gene expression may participate in the observed effects of Runx3 on axon growth. Specifically, while expression of PPP1R12C was decreased, Rock1 and Rock2

were elevated in Runx3$^{-/-}$ mice, and pharmacological inhibition of Rock activity markedly elevated axon growth of DRG neurons. One major target of Rock is NMII which is activated by Rock. NMII is thought to generate a retrograde flow of actin (Ponti *et al*, 2004; Giannone *et al*, 2007) and an inhibition of its activity decreases actin retrograde flow which increases protrusiveness (Even-Ram *et al*, 2007; Vicente-Manzanares *et al*, 2007). Inhibition of NMII activation by blebbistatin had similar effects on axon growth as Rock inhibition. These results show that early sensory neurons have ongoing Rock and NMII activities that restrict axon growth in sensory neurons. Furthermore, the proportional increased axon growth by blocking Rock activity in Runx3$^{-/-}$ neurons indicates a participation of the Rock-NMII pathway in Runx3-mediated axial differences in axon growth. One of the hallmarks of neuronal specification during development is the extensive diversification in axon morphology. Axon growth propensity encoded by position-specific transcription factors during cell-type specification may thus be an important feature shared also by other classes of neurons in the nervous system.

Materials and methods

Mouse strains

Runx3$^{-/-}$ mice and *Brn3a*$^{+/TLZ}$ mice have been described elsewhere (Levanon *et al*, 2002; Quina *et al*, 2005). *Bax*$^{-/-}$ mice were purchased from Jackson Laboratories. All experiments conformed to Swedish and European guidelines on the ethical use of animals.

In ovo electroporation

In ovo microinjections and electroporation of plasmids and siRNAs were carried out as previously described (Marmigere *et al*, 2006). The siRNA sequences were as follows: siRNA1, 5′-CCGACGG GACAGUGGUGACGGUGAU-3′ and siRNA2, 5′-UGGCGAGAUUUAAC GAUCUCCGAUU-3′. Briefly, neural tubes of HHst13–14 embryos were electroporated in ovo with pCAeGFP together with constructs of interest or siRNA and embryos were permitted to develop until indicated stages and DRG neurons from the transfected side were dissociated and cultured at low density in a minimal medium for 7 h. Runx1d is a truncated form of Runx that retains the DNA binding domain but lacks the transactivation domain, and therefore interferes with the activity of the Runx proteins (Marmigere *et al*, 2006).

In vitro cultures of whole DRG/DRG neurons and transfection

Dissociated DRG neurons were obtained after enzymatic digestion of whole DRG using collagenase/dispase (C/D, 1 mg/ml; Roche) and DNAse (0.5 mg/ml; Sigma) in N2 medium (DMEM/F12 medium with N2 supplement) with B27 supplement (Gibco). Cells were plated at low density (300 cells/well) in 24-well plates on glass coverslips precoated with poly-L-lysine (0.01%; Sigma)/laminin (10 μg/ml; R&D Systems) or matrigel when indicated (BD Bioscience). Cells were cultured in N2 medium supplemented with B27 and neurotrophins when specified: NGF, BDNF, NT3 and GDNF (each at 10 ng/ml; Promega). Axon growth was analysed after 7 h. For explant cultures, whole DRG was plated on coverslips in matrigel, a substrate that permits outgrowth of sensory axons in a neurotrophin-independent manner (Graef *et al*, 2003; Wickramasinghe *et al*, 2008; Supplementary Figure S5C and D), diluted 1:2 in DMEM-F12/glutamax medium supplemented with pen/strep, gentamicin and the pan-caspase inhibitor Q-VD-OPh (10 μM; Calbiochem). Explants were then cultured in the same medium for 14 h or 1 DIV and axons revealed by βIII-tubulin immunoreactivity. When indicated, Y27632 (a Rock inhibitor; Calbiochem) or blebbistatin (NMII inhibitor; Sigma) was added to the culture after 2 h. Images were then converted to black and white and analysed.

For the overexpression experiments, we used *in vitro* transfection of DRG neurons since expressing Runx3 in the neural tube results in a deficit of neural crest delamination. *In vitro* transfection of DRG neurons was performed as described elsewhere (Ledda *et al*, 2008) using the overexpression constructs pCARunx3 together with pCAeGFP. Cells were then plated in 24-well plates in N2 medium supplemented with B27 for 16 h without neurotrophins to allow for expression of the electroporated constructs. Thereafter, cells were lifted using C/D and replated in similar conditions. After 4 h, cultures were fixed with 4% paraformaldehyde in PBS and immunostained. Using a mouse Runx3 antibody, we observed that all GFP$^+$ neurons also successfully expressed the Runx3 overexpression construct.

For sensory neurons in culture, βIII-tubulin (Promega) staining was used to examine the full extent of axon growth of transfected (GFP$^+$) neurons. For axon length measurement, each coverslip was analysed the same way. Using a $\times 10$ objective, GFP$^+$ neurons were identified and imaged using a $\times 20$ objective. The longest axon for each identified neuron was analysed using ImageJ software program (NIH). In experiments where Runx3 expression was correlated with axon length at single cell level axon length was measured after 7 h by immunohistochemistry. For Figure 1B, images were then converted to black and white, and inverted to depict sensory neurons and their projections in black.

Analysis and quantification of these data were performed as follows. Figure 1C, $n = 12$ wells from separate experiments, with in total 269–305 neurons analysed per condition. Figure 1F, data presented as percentage of brachial, $n = 4$ samples, with DRG from at least five embryos per sample. Figure 2B, $n = 3$–4 samples for mRNA levels, with DRG from at least five embryos per sample, data presented as percentage of brachial and $n = 7$ with a total of 138–173 neurons analysed per condition for measurements of axon length in culture. In Figure 3F, $n = 10$ wells for the cultures, from separate experiments, with in total 235–268 neurons analysed per condition. In Figure 4A–D, data are expressed as percentage of control, $n = 6$–11 wells from separate experiments, with in total 86–185 neurons analysed per condition. In Figure 4E, data are expressed as percentage of control, $n = 4$ wells from separate experiments, with in total 87–103 neurons analysed per condition. In Figure 4G, data are expressed as percentage of control, $n = 6$–11 wells from separate experiments, with in total 86–185 neurons analysed per condition.

In situ hybridization, immunostaining and X-Gal staining

Embryos were fixed in 4% paraformaldehyde/PBS, cryoprotected and sectioned at 14 μm thickness. *In situ* hybridization experiments and immunostainings were performed as previously described (Marmigere *et al*, 2006). Whole-mount immunofluorescent staining was performed as previously described (Huber *et al*, 2005). The following primary antibodies were used: mouse anti-Axonin-1 (23.4-5, made by Jessell and Dodd and obtained from the Developmental Studies Hybridoma Bank), mouse anti-βIII-tubulin (Promega), mouse anti-Isl1 (39.4D5, Developmental Studies Hybridoma Bank), guinea pig anti-cRunx3 and rabbit anti-mRunx3 (Chen *et al*, 2006), goat anti-mTrkC (R&D Systems), mouse anti-neurofilament-165 kDa (2H3, made by Jessell and Dodd and obtained from the Developmental Studies Hybridoma Bank), rabbit anti-cTrkC (Lefcort *et al*, 1996) and rabbit anti-TrkA (Upstate). Secondary detection was performed with Alexa Fluor 488, 546 or 647 conjugated donkey antibodies (Invitrogen). Staining was documented by confocal microscopy (Zeiss LSM 5 *EXCITER*) using identical settings between control and experimental images. Optical sections were 2 μm in $\times 20$ overview pictures. For whole-mount staining, Z-Stacks were collected and 2D projections were created using the Zeiss LSM image processing software.

X-Gal staining was performed on paraformaldehyde fixed embryos, which were rinsed in phosphate buffer and incubated overnight in a solution containing 5 mM potassium ferrocyanide, 5 mM potassium ferricyanide, 2 mM $MgCl_2$, 1 mg/ml XGal in phosphate buffer (Hjerling-Leffler *et al*, 2005). After extensive rinsing, embryos were post-fixed with 4% paraformaldehyde, rinsed with PBS, dehydrated in methanol, cleared in BABB and photographed. For analysis of peripheral axon growth *in vivo* in Runx3$^{-/-}$, Runx3$^{-/-}$;Bax$^{-/-}$, Runx3$^{+/+}$;Bax$^{-/-}$;Brn3a$^{+/TLZ}$ and Runx3$^{-/-}$;Brax$^{-/-}$;Brn3a$^{+/TLZ}$ mice, limbs were dissected out and positioned horizontally for better visualization of the peripheral sensory axons. Measurement of axon length was performed using ImageJ software program (NIH). For *in vivo* measurements of axon growth rate, chicken embryos were collected at 6 h intervals from

HHst25 to HHSt27 and immunostained for axonin-1 as described elsewhere (Caldero *et al*, 1998). Measurements of the average distance of *in vivo* growth were conducted between thoracic and limb nerves as assessed by measuring the longest nerves in whole-mount embryos stained for Axonin-1.

Quantifications of ISH and immunostaining intensity at the cellular level were performed using ImageJ software program. Average intensity per cell (in arbitrary unit) was calculated for each section from different DRG of particular axial levels.

Limb ablation

Unilateral removal of the right hindlimb bud was performed at HHst18 as previously described (Caldero *et al*, 1998) and long before the onset of axon outgrowth. In a separate group of embryos, both the right limb bud and tail bud were removed at the same time. Operated embryos were permitted to develop to HHst26–27, the last developmental stage allowing for analysis, since at later stages target deprivation-induced cell death of DRG neuron occurs (Caldero *et al*, 1998). Analysis of PEA3, Runx3, Isl1, TrkC and CBF-b was conducted by qPCR of four samples, with DRG from at leastfour embryos per sample.

Primer design

Genbank and Ensembl cDNA sequences were used to design gene-specific primers in Primer Express 2.0 (PE Applied Biosystems) or in the Universal ProbeLibrary Assay Design Center (Roche Applied Science). Chicken homologues of the mouse TrK-C primers (Stenqvist *et al*, 2005), amplifying all extracellular domains or the intracellular tyrosine kinase domains (FL), were used. The specificity of PCR primers was determined by BLAST run of the primer sequences. All primers were purchased from MWG Biotech. Primer sequences can be found in Supplementary Table S8.

Reverse transcription

Total RNA was isolated from chicken DRGs from the indicated developmental time points and anterior-posterior axial levels, using RNeasy extraction kit (Qiagen), with in-column DNAse treatment. Total RNA was reverse transcribed with the High-Capacity cDNA Reverse Transcription Kit (Applied Biosystems), according to manufacturer's instructions. Each sample was equally divided in two tubes, a cDNA reaction tube and a negative control tube, without the reverse transcriptase (RT−). Before qPCR analysis, both cDNA and RT− samples were diluted 25 or 50 times, with DNAse/RNAse-free dH_2O (Invitrogen).

Quantitative PCR

qPCRs were performed in duplicates for each sample (with four independent samples for each developmental stage/location). Each PCR had a final volume of 25 and 5 μl of 25 × - or 50 × -diluted cDNA. RT− was run for a few samples in each run to discard genomic DNA amplification. Platinum Quantitative PCR SuperMix-UDG (Invitrogen) was used, according to manufacturer's instructions (but with a 4 × dilution from the original mastermix, instead of 2 ×). The following thermo cycling program was used: 50°C for 2 min, 94°C for 2 min and then 40 cycles of 94°C for 30 s, 59/60°C for 30 s and 72°C for 30 s on the ABI PRISM 7000 Detection System (PE Applied Biosystems, Foster City, CA, USA). A melting curve was obtained for each PCR product after each run, in order to confirm that the SYBR Green signal corresponded to a unique and specific amplicon. Random PCR products were also run in a 2–3% agarose gel to verify the size of the amplicon. Standard curves were generated for every real-time PCR run and were obtained by using serial three-fold dilutions of a sample containing the sequence of interest. Their plots were used to convert Cts (number of PCR cycles needed for a given template to be amplified to an established fluorescence threshold) into arbitrary quantities of initial template for a given sample. The expression levels were then obtained by dividing the quantity by the value of the housekeeping gene, ATPsy. ATPsy assays were run at the beginning and in the middle of assays, to verify the integrity of the samples, and also if samples had been frozen.

RNA sequencing and data analysis

Total RNA was isolated from E11.5 mouse brachial DRGs from WT or Runx3$^{-/-}$ mice (5 embryos/sample; 3 samples WT, 2 samples mutant) using Qiagen RNeasy kit and prepared for RNA sequencing using Illumina TruSeq RNA kit. A total of 163 million nucleotide reads were generated for the five samples using an Illumina Genome Analyzer IIx sequencer. Raw reads were mapped to the mouse genome using STRT software (Peter Lönnerberg and Sten Linnarsson, manuscript in preparation). Briefly, raw reads were mapped using Bowtie (Langmead *et al*, 2009). Unmapped reads were removed and the mapped reads were counted to generate a count for each genomic feature. Mapped reads were normalized using RPKM (reads per KB per million reads) normalization method (Mortazavi *et al*, 2008). For differential expression, all the values <5 were removed and the average expression level for mutant and control experiments was calculated. Upregulated and down-regulated gene lists were prepared with >1.25-fold change. For gene ontology analysis, functional enrichment was evaluated using the DAVID database http://david.abcc.ncifcrf.gov/. For differentially expressed genes, the background was set to the total list of genes present in mouse genome. Functional annotation clustering report from DAVID was used to select the top gene ontology terms. The most significant gene ontology term was selected from each cluster and the list was prepared from top gene ontology terms. Cluster enrichment score was >1 and the statistical significant threshold level for all GO terms was $P<0.05$.

Supplementary data

Supplementary data are available at *The EMBO Journal* Online (http://www.embojournal.org).

Acknowledgements

We thank Thomas Jessell, Albert Chen, Silvia Arber and Louis Reichardt for generously providing antibodies against chicken and mouse Runx3, ER81 and PEA3, and chicken TrkC, respectively. We also thank Helena Samuelsson for her technical support. This work was supported by the Swedish Medical Research Council, Knut and Alice Wallenbergs Foundation (for CLICK imaging facility), the Swedish foundation for strategic research and Linné grants (CEDB and DBRM grants), the Swedish Brain Foundation, Hållsten Foundation, EU FP7 MOLPARK collaborative project and ERC advanced grant (232675) to PE, by Israel Science Foundation (ISF) BioMed program to YG and by the Swedish Medical Research Council, Karolinska Institute, Åke Wiberg foundation and the European Union to FL.

Author contributions: FL and PE designed and supervised the study. FL performed most of the experiments, analysed the data and prepared the figures. US, SH-L, JB, GCB, IS, CV, DL, YW, MCMF, OK and IA performed some experiments. DL, YG and ET developed and provided mutant mice. FL and PE wrote the paper, with input from all co-authors.

Conflict of interest

The authors declare that they have no conflict of interest.

References

Arber S, Ladle DR, Lin JH, Frank E, Jessell TM (2000) ETS gene Er81 controls the formation of functional connections between group Ia sensory afferents and motor neurons. *Cell* **101:** 485–498

Bachy I, Franck MC, Li L, Abdo H, Pattyn A, Ernfors P (2011) The transcription factor Cux2 marks development of an A-delta sublineage of TrkA sensory neurons. *Dev Biol* **360:** 77–86

Bae SC, Ogawa E, Maruyama M, Oka H, Satake M, Shigesada K, Jenkins NA, Gilbert DJ, Copeland NG, Ito Y (1994) PEBP2 alpha B/mouse AML1 consists of multiple isoforms that possess differential transactivation potentials. *Mol Cell Biol* **14:** 3242–3252

Bannert N, Vollhardt K, Asomuddinov B, Haag M, Konig H, Norley S, Kurth R (2003) PDZ Domain-mediated interaction of

interleukin-16 precursor proteins with myosin phosphatase targeting subunits. *J Biol Chem* **278:** 42190–42199

Caldero J, Prevette D, Mei X, Oakley RA, Li L, Milligan C, Houenou L, Burek M, Oppenheim RW (1998) Peripheral target regulation of the development and survival of spinal sensory and motor neurons in the chick embryo. *J Neurosci* **18:** 356–370

Chen AI, de Nooij JC, Jessell TM (2006) Graded activity of transcription factor Runx3 specifies the laminar termination pattern of sensory axons in the developing spinal cord. *Neuron* **49:** 395–408

Conde C, Caceres A (2009) Microtubule assembly, organization and dynamics in axons and dendrites. *Nat Rev Neurosci* **10:** 319–332

Davies AM (1989) Intrinsic differences in the growth rate of early nerve fibres related to target distance. *Nature* **337:** 553–555

De Marco Garcia NV, Jessell TM (2008) Early motor neuron pool identity and muscle nerve trajectory defined by postmitotic restrictions in Nkx6.1 activity. *Neuron* **57:** 217–231

Dickson BJ (2002) Molecular mechanisms of axon guidance. *Science* **298:** 1959–1964

Ernfors P, Lee KF, Kucera J, Jaenisch R (1994) Lack of neurotrophin-3 leads to deficiencies in the peripheral nervous system and loss of limb proprioceptive afferents. *Cell* **77:** 503–512

Even-Ram S, Doyle AD, Conti MA, Matsumoto K, Adelstein RS, Yamada KM (2007) Myosin IIA regulates cell motility and actomyosin-microtubule crosstalk. *Nat Cell Biol* **9:** 299–309

Genc B, Ozdinler PH, Mendoza AE, Erzurumlu RS (2004) A chemoattractant role for NT-3 in proprioceptive axon guidance. *PLoS Biol* **2:** e403

Giannone G, Dubin-Thaler BJ, Rossier O, Cai Y, Chaga O, Jiang G, Beaver W, Dobereiner HG, Freund Y, Borisy G, Sheetz MP (2007) Lamellipodial actin mechanically links myosin activity with adhesion-site formation. *Cell* **128:** 561–575

Graef IA, Wang F, Charron F, Chen L, Neilson J, Tessier-Lavigne M, Crabtree GR (2003) Neurotrophins and netrins require calcineurin/NFAT signaling to stimulate outgrowth of embryonic axons. *Cell* **113:** 657–670

Guan W, Puthenveedu MA, Condic ML (2003) Sensory neuron subtypes have unique substratum preference and receptor expression before target innervation. *J Neurosci* **23:** 1781–1791

Hippenmeyer S, Shneider NA, Birchmeier C, Burden SJ, Jessell TM, Arber S (2002) A role for neuregulin1 signaling in muscle spindle differentiation. *Neuron* **36:** 1035–1049

Hjerling-Leffler J, Marmigere F, Heglind M, Cederberg A, Koltzenburg M, Enerback S, Ernfors P (2005) The boundary cap: a source of neural crest stem cells that generate multiple sensory neuron subtypes. *Development* **132:** 2623–2632

Honig MG, Frase PA, Camilli SJ (1998) The spatial relationships among cutaneous, muscle sensory and motoneuron axons during development of the chick hindlimb. *Development* **125:** 995–1004

Huang da W, Sherman BT, Tan Q, Collins JR, Alvord WG, Roayaei J, Stephens R, Baseler MW, Lane HC, Lempicki RA (2007a) The DAVID Gene Functional Classification Tool: a novel biological module-centric algorithm to functionally analyze large gene lists. *Genome Biol* **8:** R183

Huang da W, Sherman BT, Tan Q, Kir J, Liu D, Bryant D, Guo Y, Stephens R, Baseler MW, Lane HC, Lempicki RA (2007b) DAVID Bioinformatics Resources: expanded annotation database and novel algorithms to better extract biology from large gene lists. *Nucleic Acids Res* **35:** W169–W175

Huber AB, Kania A, Tran TS, Gu C, De Marco Garcia N, Lieberam I, Johnson D, Jessell TM, Ginty DD, Kolodkin AL (2005) Distinct roles for secreted semaphorin signaling in spinal motor axon guidance. *Neuron* **48:** 949–964

Huber AB, Kolodkin AL, Ginty DD, Cloutier JF (2003) Signaling at the growth cone: ligand-receptor complexes and the control of axon growth and guidance. *Annu Rev Neurosci* **26:** 509–563

Inoue K, Ozaki S, Shiga T, Ito K, Masuda T, Okado N, Iseda T, Kawaguchi S, Ogawa M, Bae SC, Yamashita N, Itohara S, Kudo N, Ito Y (2002) Runx3 controls the axonal projection of proprioceptive dorsal root ganglion neurons. *Nat Neurosci* **5:** 946–954

Jacobson M, Huang S (1985) Neurite outgrowth traced by means of horseradish peroxidase inherited from neuronal ancestral cells in frog embryos. *Dev Biol* **110:** 102–113

Kania A, Johnson RL, Jessell TM (2000) Coordinate roles for LIM homeobox genes in directing the dorsoventral trajectory of motor axons in the vertebrate limb. *Cell* **102:** 161–173

Kovacs M, Toth J, Hetenyi C, Malnasi-Csizmadia A, Sellers JR (2004) Mechanism of blebbistatin inhibition of myosin II. *J Biol Chem* **279:** 35557–35563

Kramer ER, Knott L, Su F, Dessaud E, Krull CE, Helmbacher F, Klein R (2006a) Cooperation between GDNF/Ret and ephrinA/EphA4 signals for motor-axon pathway selection in the limb. *Neuron* **50:** 35–47

Kramer I, Sigrist M, de Nooij JC, Taniuchi I, Jessell TM, Arber S (2006b) A role for Runx transcription factor signaling in dorsal root ganglion sensory neuron diversification. *Neuron* **49:** 379–393

Kucera J, Fan G, Jaenisch R, Linnarsson S, Ernfors P (1995) Dependence of developing group Ia afferents on neurotrophin-3. *J Comp Neurol* **363:** 307–320

Langmead B, Trapnell C, Pop M, Salzberg SL (2009) Ultrafast and memory-efficient alignment of short DNA sequences to the human genome. *Genome Biol* **10:** R25

Lawson SN, Biscoe TJ (1979) Development of mouse dorsal root ganglia: an autoradiographic and quantitative study. *J Neurocytol* **8:** 265–274

Ledda F, Bieraugel O, Fard SS, Vilar M, Paratcha G (2008) Lrig1 is an endogenous inhibitor of Ret receptor tyrosine kinase activation, downstream signaling, and biological responses to GDNF. *J Neurosci* **28:** 39–49

Lefcort F, Clary DO, Rusoff AC, Reichardt LF (1996) Inhibition of the NT-3 receptor TrkC, early in chick embryogenesis, results in severe reductions in multiple neuronal subpopulations in the dorsal root ganglia. *J Neurosci* **16:** 3704–3713

Levanon D, Bettoun D, Harris-Cerruti C, Woolf E, Negreanu V, Eilam R, Bernstein Y, Goldenberg D, Xiao C, Fliegauf M, Kremer E, Otto F, Brenner O, Lev-Tov A, Groner Y (2002) The Runx3 transcription factor regulates development and survival of TrkC dorsal root ganglia neurons. *EMBO J* **21:** 3454–3463

Lin JH, Saito T, Anderson DJ, Lance-Jones C, Jessell TM, Arber S (1998) Functionally related motor neuron pool and muscle sensory afferent subtypes defined by coordinate ETS gene expression. *Cell* **95:** 393–407

Lumsden AG, Davies AM (1983) Earliest sensory nerve fibres are guided to peripheral targets by attractants other than nerve growth factor. *Nature* **306:** 786–788

Luria V, Krawchuk D, Jessell TM, Laufer E, Kania A (2008) Specification of motor axon trajectory by ephrin-B:EphB signaling: symmetrical control of axonal patterning in the developing limb. *Neuron* **60:** 1039–1053

Marmigere F, Ernfors P (2007) Specification and connectivity of neuronal subtypes in the sensory lineage. *Nat Rev Neurosci* **8:** 114–127

Marmigere F, Montelius A, Wegner M, Groner Y, Reichardt LF, Ernfors P (2006) The Runx1/AML1 transcription factor selectively regulates development and survival of TrkA nociceptive sensory neurons. *Nat Neurosci* **9:** 180–187

Meyers S, Lenny N, Hiebert SW (1995) The t(8;21) fusion protein interferes with AML-1B-dependent transcriptional activation. *Mol Cell Biol* **15:** 1974–1982

Montelius A, Marmigere F, Baudet C, Aquino JB, Enerback S, Ernfors P (2007) Emergence of the sensory nervous system as defined by Foxs1 expression. *Differentiation* **75:** 404–417

Moret F, Renaudot C, Bozon M, Castellani V (2007) Semaphorin and neuropilin co-expression in motoneurons sets axon sensitivity to environmental semaphorin sources during motor axon pathfinding. *Development* **134:** 4491–4501

Mortazavi A, Williams BA, McCue K, Schaeffer L, Wold B (2008) Mapping and quantifying mammalian transcriptomes by RNA-Seq. *Nat Methods* **5:** 621–628

O'Donnell M, Chance RK, Bashaw GJ (2009) Axon growth and guidance: receptor regulation and signal transduction. *Annu Rev Neurosci* **32:** 383–412

Patel TD, Jackman A, Rice FL, Kucera J, Snider WD (2000) Development of sensory neurons in the absence of NGF/TrkA signaling *in vivo*. *Neuron* **25:** 345–357

Patel TD, Kramer I, Kucera J, Niederkofler V, Jessell TM, Arber S, Snider WD (2003) Peripheral NT3 signaling is required for ETS protein expression and central patterning of proprioceptive sensory afferents. *Neuron* **38:** 403–416

Polleux F, Snider W (2010) Initiating and growing an axon. *Cold Spring Harb Perspect Biol* **2:** a001925

Ponti A, Machacek M, Gupton SL, Waterman-Storer CM, Danuser G (2004) Two distinct actin networks drive the protrusion of migrating cells. *Science* **305:** 1782–1786

Quina LA, Pak W, Lanier J, Banwait P, Gratwick K, Liu Y, Velasquez T, O'Leary DD, Goulding M, Turner EE (2005) Brn3a-expressing retinal ganglion cells project specifically to thalamocortical and collicular visual pathways. *J Neurosci* **25:** 11595–11604

Sharma K, Leonard AE, Lettieri K, Pfaff SL (2000) Genetic and epigenetic mechanisms contribute to motor neuron pathfinding. *Nature* **406:** 515–519

Sherman BT, Huang da W, Tan Q, Guo Y, Bour S, Liu D, Stephens R, Baseler MW, Lane HC, Lempicki RA (2007) DAVID Knowledgebase: a gene-centered database integrating heterogeneous gene annotation resources to facilitate high-throughput gene functional analysis. *BMC Bioinformatics* **8:** 426

Stenqvist A, Agerman K, Marmigere F, Minichiello L, Ernfors P (2005) Genetic evidence for selective neurotrophin 3 signalling through TrkC but not TrkB *in vivo*. *EMBO Rep* **6:** 973–978

Tanaka E, Ho T, Kirschner MW (1995a) The role of microtubule dynamics in growth cone motility and axonal growth. *J Cell Biol* **128:** 139–155

Tanaka EM, Kirschner MW (1991) Microtubule behavior in the growth cones of living neurons during axon elongation. *J Cell Biol* **115:** 345–363

Tanaka T, Tanaka K, Ogawa S, Kurokawa M, Mitani K, Nishida J, Shibata Y, Yazaki Y, Hirai H (1995b) An acute myeloid leukemia gene, AML1, regulates hemopoietic myeloid cell differentiation and transcriptional activation antagonistically by two alternative spliced forms. *EMBO J* **14:** 341–350

Vicente-Manzanares M, Ma X, Adelstein RS, Horwitz AR (2009) Non-muscle myosin II takes centre stage in cell adhesion and migration. *Nature reviews. Mol Cell Biol* **10:** 778–790

Vicente-Manzanares M, Zareno J, Whitmore L, Choi CK, Horwitz AF (2007) Regulation of protrusion, adhesion dynamics, and polarity by myosins IIA and IIB in migrating cells. *J Cell Biol* **176:** 573–580

Wang G, Scott SA (2000) The 'waiting period' of sensory and motor axons in early chick hindlimb: its role in axon pathfinding and neuronal maturation. *J Neurosci* **20:** 5358–5366

White FA, Keller-Peck CR, Knudson CM, Korsmeyer SJ, Snider WD (1998) Widespread elimination of naturally occurring neuronal death in Bax-deficient mice. *J Neurosci* **18:** 1428–1439

Wickramasinghe SR, Alvania RS, Ramanan N, Wood JN, Mandai K, Ginty DD (2008) Serum response factor mediates NGF-dependent target innervation by embryonic DRG sensory neurons. *Neuron* **58:** 532–545